NRC Research Press

ARTICLE

Study of the boundary layer heat transfer of nanofluids over a stretching sheet: Passive control of nanoparticles at the surface

M. Ghalambaz, E. Izadpanahi, A. Noghrehabadi, and A. Chamkha

Abstract: The boundary layer heat and mass transfer of nanofluids over an isothermal stretching sheet is analyzed using a drift-flux model. The relative slip velocity between the nanoparticles and the base fluid is taken into account. The nanoparticles' volume fractions at the surface of the sheet are considered to be adjusted passively. The thermal conductivity and the dynamic viscosity of the nanofluid are considered as functions of the local volume fraction of the nanoparticles. A non-dimensional parameter, heat transfer enhancement ratio, is introduced, which shows the alteration of the thermal convective coefficient of the nanofluid compared to the base fluid. The governing partial differential equations are reduced into a set of nonlinear ordinary differential equations using appropriate similarity transformations and then solved numerically using the fourth-order Runge–Kutta and Newton–Raphson methods along with the shooting technique. The effects of six non-dimensional parameters, namely, the Prandtl number of the base fluid Pr_{bf}, Lewis number Le, Brownian motion parameter Nb, thermophoresis parameter Nt, variable thermal conductivity parameter Nc and the variable viscosity parameter Nv, on the velocity, temperature, and concentration profiles as well as the reduced Nusselt number and the enhancement ratio are investigated. Finally, case studies for Al_2O_3 and Cu nanoparticles dispersed in water are performed. It is found that increases in the ambient values of the nanoparticles volume fraction cause decreases in both the dimensionless shear stress $f''(0)$ and the reduced Nusselt number Nur. Furthermore, an augmentation of the ambient value of the volume fraction of nanoparticles results in an increase the heat transfer enhancement ratio h_{nf}/h_{bf}. Therefore, using nanoparticles produces heat transfer enhancement from the sheet.

PACS Nos.: 44.20.+b, 44.27.+g.

Résumé : Nous utilisons un modèle de flux de dérive (drift-flux) pour analyser le transfert de chaleur et de masse de la couche limite d'un nanofluide sur une plaque isotherme étirable. Nous tenons compte de la vitesse de glissement entre les nanoparticules et le fluide de base. Nous considérons que la fraction volumique des nanoparticules à la surface de la plaque est ajustée passivement et prenons pour acquis que la conductivité thermique et la viscosité dynamique du nanofluide sont fonction de la valeur locale de la fraction de nanoparticules. Nous introduisons un paramètre sans dimension, le rapport d'augmentation du transfert de chaleur, qui montre le changement de valeur du coefficient thermique convectif, entre le nanofluide et le fluide de base. Des transformations de similarité appropriées réduisent les équations directrices aux dérivées partielles en un ensemble d'équations différentielles ordinaires non linéaires qui sont alors solutionnées numériquement en utilisant la méthode de Runge–Kutta au quatrième ordre avec celle de Newton–Raphson et une technique de tir. Nous étudions comment la vitesse, les profils de température et de concentration, le nombre réduit de Nusselt et le rapport d'augmentation, sont affectés par les valeurs des six principaux paramètres sans dimension que sont le nombre de Prandtl du fluide de base Pr_{bf}, le nombre de Lewis Le, le paramètre du mouvement brownien Nb, le paramètre de thermophorèse Nt, le paramètre de conductivité thermique variable Nc et le paramètre de viscosité variable Nv. Nous étudions les cas de nanoparticules de Al_2O_3 et de Cu dans l'eau. Nous trouvons que l'augmentation de la valeur ambiante de la fraction des nanoparticules amène une diminution de la contrainte de cisaillement sans dimension $f''(0)$ et du nombre réduit de Nusselt Nur. De plus, elle cause aussi une augmentation du rapport d'augmentation du transfert de chaleur h_{nf}/h_{bf}. Conséquemment, les nanoparticules causent une augmentation du transfert de chaleur venant de la plaque. [Traduit par le Rédaction]

1. Introduction

The fluid flow and heat transfer over a stretching sheet is an important problem in many industries. There are numerous industrial applications for a stretching sheet, such as extrusion of plastics, paper production, metal spinning, wire drawing, glass blowing, hot rolling, manufacture of rubber sheets, polymer engineering, cooling of metallic sheets, and crystal growing [1–3]. As an example, in extrusion of plastics, the molten plastic is stretched through a slit to shape a desired form while it is subjected to a cooling liquid. The stretching process is utilized to produce products, such as sheets, plates, and flexible films for bags and packaging purposes.

Crane [4] was the first who investigated the problem of fluid flow and heat transfer in a boundary layer over a stretching sheet. After the pioneering work of Crane [4], the problem of laminar boundary layer over a stretching sheet is considered by many researchers and a great amount of literature has been generated.

A nanofluid is described as being synthesized from a low thermal conductivity base fluid and dispersed solid nanoparticles with high thermal conductivity and nanometre length scales. The nanoparticles used in nanofluids are typically made of metals (Al, Cu), oxides of metals (Al_2O_3), carbides (SiC), nitrides (AlN, SiN), or nonmetals (graphite, carbon nanotubes). The diameter range of

Received 3 July 2014. Accepted 1 December 2014.

M. Ghalambaz. Department of Mechanical Engineering, Dezful Branch, Islamic Azad University, Dezful, Iran.
E. Izadpanahi and A. Noghrehabadi. Department of Mechanical Engineering, Shahid Chamran University of Ahvaz, Ahvaz, Iran.
A. Chamkha. Mechanical Engineering Department, Prince Mohammad Bin Fahd University, Al-Khobar 31952, Kingdom of Saudi Arabia.
Corresponding author: Mohammad Ghalambaz (e-mail: m.ghalambaz@iaud.ac.ir).

nanoparticles is between 1 and 100 nm. Nanofluids commonly contain 5% or lower volume fraction of nanoparticles. One of the outstanding characteristics of nanofluids is the thermal conductivity enhancement. For example, it was reported that the effective thermal conductivity of an ethylene–glycol-based nanofluid, which contains nano-size copper particles with diameters less than 10 nm increased by up to 40 at 0.3% volume of dispersed particles [5]. Comprehensive references on this subject can be found in the recently published book by Das et al. [6] and in the papers by Wang and Mujumdar [7], Kakaç and Pramuanjaroenkij [8], Chandrasekar et al. [9], and Wu and Zhao [10].

In industrial processes, such as extrusion of plastics, the quality of the final product strongly depends on the heat transfer rate from the surface of the product. Any increase of heat transfer from the sheet would significantly affect the quality of the product. The thermal conductivity of the conventional working fluids, such as water, oil, and ethylene glycol, is very low; hence the nanofluids are proposed as a means to increase the thermal conductivity of these base fluids.

Very recently, Khan and Pop [11] analyzed the boundary-layer flow of a nanofluid past a stretching sheet using a model in which the Brownian motion and the thermophoresis effects are taken into account. They reduced the whole governing partial differential equations in to a set of nonlinear ordinary differential equations and solved them numerically. Following the work of Khan and Pop [11], the set of ordinary differential equations was solved by Hassani et al. [12] using the homotopy analysis method. After that, many researchers have extended the work and considered heat transfer of nanofluids over stretching sheets and examined other effects, such as the thermal radiation and magnetic field effects [13], a convective boundary condition [14], a nonlinear stretching velocity [15], a partial-slip boundary condition [16], the presence of a magnetic field [17], partial-slip and convective boundary conditions [18], heat generation–absorption effect [19], non-Newtonian effects [20, 21], and in the presence of a porous medium [22], variable thermal conductivity [23]. In a recent paper by Noghrehabadi et al. [24], the range of non-dimensional parameters of nanofluids has been discussed.

In all of the mentioned studies [11–24], the nanoparticle concentration was assumed to be constant and controlled actively on the surface of the sheet. Accordingly, there is a mass flux of nanoparticles through the surface, and hence, the Sherwood number is not zero. However, it is not clear how the concentration can be maintained constant at the surface. Very recently, Kuznetsov and Nield [25] proposed a new practical boundary condition for nanofluids. They have adopted a zero mass flux condition of nanoparticles through the surface and allowed the volume fraction of nanoparticles to adjust at the surface passively. Additionally, this new boundary condition for concentration of nanoparticles is considered by other researchers over the stretching sheet. Rahman et al. [26] studied the effects of nanofluid over a permeable exponentially shrinking–stretching surface with second-order slip velocity, when the boundary condition of nanoparticle concentration over the surface of the sheet is passively controlled. Similarly, Rizwan et al. [27] utilized this boundary condition over a stretching sheet in the presence of a magnetic field, thermal radiation, and slip effects.

The previous studies [11–22] assumed that the dynamic viscosity and the thermal conductivity of nanofluids are exclusively functions of the ambient volume fraction of nanoparticles and the effect of the local volume fraction of nanoparticles on the thermophysical properties was completely neglected. However, it is clear that the thermo-physical properties of nanofluids are strongly affected by the volume fraction of nanoparticles [28–30]. The experimental studies demonstrate that the thermal conductivity of a nanofluid is an increasing function of the volume fraction of nanoparticles. As an example, the experimental studies [31–34] for Al_2O_3–water nanofluid revealed that the thermal conductivity of an Al_2O_3–water nanofluid was an increasing function of the volume fraction of nanoparticles such that an increase of nanoparticles volume fraction from 1% to 3% increased the thermal conductivity of the nanofluid from 3.43% to 9.7%. It was concluded that the thermal conductivity of nanofluids increased linearly with increasing values of the nanoparticles volume fraction [34, 35]. In addition, the dynamic viscosity of nanofluids was also found to be an increasing function of the nanoparticle volume fraction [31, 34, 36, 37].

Fig. 1. Schematic view of coordinate system and stretching sheet.

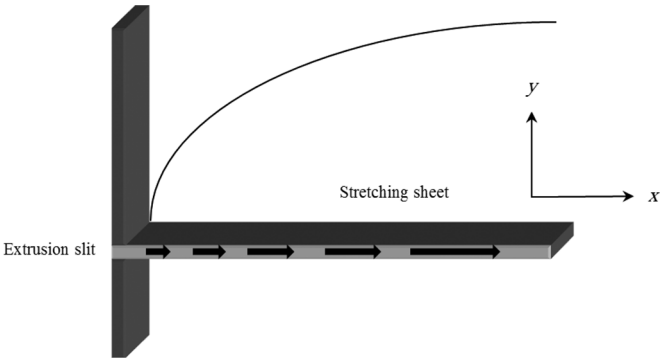

The aim of the present study is to probe the fluid flow and heat transfer of nanofluids caused by a stretching sheet. It is assumed that the dynamic viscosity and the thermal conductivity of the nanofluid are functions of the local volume fraction of nanoparticles. In addition, the concentration of nanoparticles at the surface of the sheet is adjusted passively by the boundary layer. This makes the model more practical and more realistic for nanofluid applications. The governing partial differential equations are transformed into a set of nonlinear ordinary differential equations by using similarity variables. The governing equations depend on six non-dimensional parameters, namely, the Prandtl number of the base fluid Pr_{bf}, Lewis number Le, Brownian motion parameter Nb, thermophoresis parameter Nt, variable thermal conductivity parameter Nc, and the variable viscosity parameter Nv. Finally, the practical ranges of these six parameters for water as a base fluid and Al_2O_3 and Cu as the dispersed nanoparticles are carried out. To the best of the authors' knowledge, the results of the present study are new and have not been published before.

2. Formulation of the problem

Consider the two-dimensional laminar steady flow of an incompressible nanofluid caused by a stretching sheet, where the *x*-axis is measured along the sheet and the *y*-axis is measured normal to the sheet. The physical model and the coordinate system are presented in Fig. 1. It is assumed that the sheet is at constant temperature T_w. The temperature and the volume fraction of nanoparticles outside the boundary layer (ambient) are constant and are denoted T_∞ and C_∞, respectively. The viscosity and the thermal conductivity of the nanofluid are assumed functions of the local volume fraction of nanoparticles. It is assumed that the nanofluid is a dilute mixture of nanoparticles. As the thermal conductivity of nanoparticles is higher than the thermal conductivity of the base fluid, and the nanoparticles are also very fine, it can be assumed that the nanoparticles and the base fluid are in local thermal equilibrium. The nanoparticle materials are commonly chosen for their chemical inertness with the base fluid. The base fluid is also a pure fluid; therefore, there is no chemical reaction or heat generation in the boundary layer. Buongiorno et al. [38] and Venerus et al. [39] demonstrated that most nanofluids show a Newtonian fluid behavior. Following the work of Buongiorno [28], the basic steady-state equations for the balance laws of

mass, momentum, thermal energy, and nanoparticle concentration are written for a Newtonian nanofluid as follows:

$$\frac{\partial u}{\partial x}+\frac{\partial v}{\partial y}=0 \tag{1}$$

$$u\frac{\partial u}{\partial x}+v\frac{\partial u}{\partial y}=\frac{1}{\rho_{\mathrm{nf},\infty}}\left[\frac{\partial}{\partial x}\left(\mu_{\mathrm{nf}}\frac{\partial u}{\partial x}\right)+\frac{\partial}{\partial y}\left(\mu_{\mathrm{nf}}\frac{\partial u}{\partial y}\right)\right] \tag{2}$$

$$u\frac{\partial v}{\partial x}+v\frac{\partial v}{\partial y}=\frac{1}{\rho_{\mathrm{nf},\infty}}\left[\frac{\partial}{\partial x}\left(\mu_{\mathrm{nf}}\frac{\partial v}{\partial x}\right)+\frac{\partial}{\partial y}\left(\mu_{\mathrm{nf}}\frac{\partial v}{\partial y}\right)\right] \tag{3}$$

$$u\frac{\partial T}{\partial x}+v\frac{\partial T}{\partial y}=\frac{1}{(\rho c)_{\mathrm{nf},\infty}}\left[\frac{\partial}{\partial x}\left(k_{\mathrm{nf}}\frac{\partial T}{\partial x}\right)+\frac{\partial}{\partial y}\left(k_{\mathrm{nf}}\frac{\partial T}{\partial y}\right)\right]+\frac{(\rho c)_{\mathrm{p}}}{(\rho c)_{\mathrm{nf},\infty}}\left\{D_{\mathrm{B}}\left(\frac{\partial T}{\partial x}\frac{\partial C}{\partial x}+\frac{\partial T}{\partial y}\frac{\partial C}{\partial y}\right)+\frac{D_{\mathrm{T}}}{T_\infty}\left[\left(\frac{\partial T}{\partial x}\right)^2+\left(\frac{\partial T}{\partial y}\right)^2\right]\right\} \tag{4}$$

$$u\frac{\partial C}{\partial x}+v\frac{\partial C}{\partial y}=D_{\mathrm{B}}\left(\frac{\partial^2 C}{\partial x^2}+\frac{\partial^2 C}{\partial y^2}\right)+\frac{D_{\mathrm{T}}}{T_\infty}\left(\frac{\partial^2 T}{\partial x^2}+\frac{\partial^2 T}{\partial y^2}\right) \tag{5}$$

The boundary conditions at the surface of the impermeable sheet and far from the sheet are, respectively, written as:

$$u=u_{\mathrm{w}}\quad v=0\quad T=T_{\mathrm{w}}\quad D_{\mathrm{B}}\frac{\partial C}{\partial y}+\frac{D_{\mathrm{T}}}{T_\infty}\frac{\partial T}{\partial y}=0\quad\text{at}\quad y=0 \tag{6}$$

$$u=0\quad T=T_\infty\quad C=C_\infty\quad\text{at}\quad y\to\infty \tag{7}$$

where u and v are the velocity components along the x-axis and y-axis, respectively; T is the temperature of the nanofluid mixture; C is the volume fraction of nanoparticles; $\rho_{\mathrm{nf},\infty}$ is the density of the nanofluid; D_{B} is the Brownian diffusion coefficient; D_{T} is the thermophoretic diffusion coefficient; $(\rho c)_{\mathrm{p}}$ is the effective heat capacity of the nanoparticles; and $(\rho c)_{\mathrm{nf},\infty}$ is the heat capacity of the nanofluid.

According to the experimental investigations [28–37], the dynamic viscosity and the thermal conductivity of nanofluids are considered as increasing functions of the volume fraction of nanoparticles. It is assumed that these functions have linear relations with the nanoparticle volume fraction

$$\frac{k_{\mathrm{nf}}}{k_{\mathrm{nf},\infty}}=1+\mathrm{Nc}\frac{(C-C_\infty)}{C_\infty} \tag{8}$$

$$\frac{\mu_{\mathrm{nf}}}{\mu_{\mathrm{nf},\infty}}=1+\mathrm{Nv}\frac{(C-C_\infty)}{C_\infty} \tag{9}$$

where $\mu_{\mathrm{nf},\infty}$ and $k_{\mathrm{nf},\infty}$ are the viscosity and the thermal conductivity, respectively, of the nanofluid outside the boundary layer; and Nc and Nv denote the variable thermal conductivity parameter and variable viscosity parameter, respectively. Now, the dimensionless functions f, θ, and ϕ and the similarity variable, η, are introduced as follows:

$$\eta=\left(\frac{a}{\upsilon_{\mathrm{nf},\infty}}\right)^{1/2}y\qquad\psi=(a\upsilon_{\mathrm{nf},\infty})^{1/2}xf(\eta)$$
$$\theta=\frac{T-T_\infty}{T_{\mathrm{w}}-T_\infty}\qquad\phi=\frac{C-C_\infty}{C_\infty} \tag{10}$$

where f, θ, and ϕ denote the dimensionless velocity, temperature, and concentration of nanoparticles, respectively. By substituting (10) into (1)–(5), the transformed momentum, energy, and concentration of nanoparticles are obtained as follows:

$$(1+\mathrm{Nv}\phi)f'''+(\mathrm{Nv}\phi'+f)f''-f'^2=0 \tag{11}$$

$$(1+\mathrm{Nc}\phi)\theta''+(\mathrm{Nc}\phi'+\mathrm{Pr}_{\mathrm{nf}}f+\mathrm{Pr}_{\mathrm{nf}}\mathrm{Nb}\phi'+\mathrm{Pr}_{\mathrm{nf}}\mathrm{Nt}\theta')\theta'=0 \tag{12}$$

$$\phi''+\mathrm{Le}f\phi'+\frac{\mathrm{Nt}}{\mathrm{Nb}}\theta''=0 \tag{13}$$

Similarly, the non-dimensional boundary conditions are obtained as follows:

$$f'=1\quad f=0\quad\theta=1\quad\mathrm{Nb}\phi'+\mathrm{Nt}\theta'=0\quad\text{at}\quad\eta=0 \tag{14}$$

$$f'=0\quad\theta=0\quad\phi=0\quad\text{at}\quad\eta\to\infty \tag{15}$$

where the parameters Le, Nb, and Nt are defined as

$$\mathrm{Le}=\frac{\upsilon_{\mathrm{nf},\infty}}{D_{\mathrm{B}}}\qquad\mathrm{Nb}=\frac{(\rho c)_{\mathrm{p}}D_{\mathrm{B}}C_\infty}{(\rho c)_{\mathrm{nf}}\upsilon_{\mathrm{nf},\infty}}\qquad\mathrm{Nt}=\frac{(\rho c)_{\mathrm{p}}D_{\mathrm{T}}(T_w-T_\infty)}{(\rho c)_{\mathrm{nf}}T_\infty\upsilon_{\mathrm{nf},\infty}} \tag{16}$$

where Le, Nb, and Nt denote the nanofluid Lewis number, Brownian motion parameter, and the thermophoresis parameter, respectively. Assuming $C=0$, (8) and (9) approximate the thermal conductivity and the dynamic viscosity of the base fluid as $k_{\mathrm{bf}}/k_{\mathrm{nf},\infty}=1-\mathrm{Nc}$ and $\mu_{\mathrm{bf}}/\mu_{\mathrm{nf},\infty}=1-\mathrm{Nv}$. Hence, the Prandtl number of the nanofluid can be written as a function of the Prandtl number of the base fluid as

$$\mathrm{Pr}_{\mathrm{nf}}=\mathrm{Pr}_{\mathrm{bf}}\left(\frac{1-\mathrm{Nc}}{1-\mathrm{Nv}}\right)\frac{c_{\mathrm{nf}}}{c_{\mathrm{bf}}} \tag{17}$$

Assuming the practical case of an Al_2O_3–water nanofluid with a comparatively high volume fraction of nanoparticles, $C_\infty=5.0\%$, the ratio $c_{\mathrm{nf}}/c_{\mathrm{bf}}$ is evaluated as 0.96. Hence, for convenience, the ratio $c_{\mathrm{nf}}/c_{\mathrm{bf}}$ is assumed to be unity in future calculations. Moreover, the important non-dimensional parameter of heat transfer, the Nusselt number, is introduced as follows:

$$\mathrm{Nu}_x=\frac{q_{\mathrm{W}}x}{k_{\mathrm{nf},\infty}(T_{\mathrm{W}}-T_\infty)} \tag{18}$$

where q_{W} is the wall heat flux, introduced as $q_{\mathrm{W}}=-k_{\mathrm{nf,w}}\partial T/\partial y$ at $y=0$; and $k_{\mathrm{nf,w}}=k_{\mathrm{nf},\infty}[1+(C_{\mathrm{W}}-C_\infty)/C_\infty]$. Using the dimensionless parameters, (18) becomes

$$\mathrm{Nu}_x\mathrm{Re}_{\mathrm{nf},x}^{-1/2}=-[1+\mathrm{Nc}\phi(0)]\theta'_{\mathrm{nf}}(0) \tag{19}$$

The value of $\mathrm{Nu}_x\mathrm{Re}_{\mathrm{nf},x}^{-1/2}$ is introduced as the reduced Nusselt number Nur. Considering a conventional base fluid, the thermophysical properties (thermal conductivity and dynamic viscosity) are constant, and hence, Nu_x is solely a function of the temperature gradient ($\theta'(0)$) at the surface. Thus, any increase or decrease of Nu_x would indicate an enhancement or a reduction, respectively, of heat transfer from the surface. However, in the case of nanofluids, the thermo-physical properties are functions of the nanoparticle volume fraction. Hence, the reduced Nusselt number in the nanofluid is generally a function of the temperature gradient at the surface [$\theta'(0)$], the thermal conductivity and dynamic viscosity of the nanofluid, and other thermo-physical properties. Therefore, it is clear that the augmentation or reduction of

the reduced Nusselt number cannot directly show the enhancement or deterioration of heat transfer from the surface. Here, in the present study, we have introduced the heat transfer enhancement ratio as

$$\frac{h_{nf}}{h_{bf}} = (1 - Nv)^{1/2}\frac{1 + Nc\phi(0)}{1 - Nc}\frac{\theta'_{nf}(0)}{\theta'_{bf}(0)}\left(\frac{\rho_{nf}}{\rho_{bf}}\right)^{1/2} \quad (20)$$

The heat transfer enhancement ratio simply compares the convective heat transfer induced by using the nanofluid to the convective heat transfer induced by the original base fluid. Because the temperature of the surface (T_w) and the ambient temperature (T_∞) in both cases of the nanofluid and the base fluid are the same, the convective heat transfer coefficient (h) indicates the heat transfer rate from the surface. Any increase of h_{nf} in comparison with h_{bf} would show the heat transfer enhancement of using nanoparticles in comparison with using the original base fluid.

3. Result and discussion

The set of nonlinear ordinary differential equations (11)–(13) subject to boundary conditions (14) and (15) are solved numerically using the fourth-order Runge–Kutta and the Newton–Raphson methods along with a systematic guessing of $f''0)$, $\theta'(0)$, and $\phi(0)$ by the shooting technique. The effects of the non-dimensional parameters, such as, Pr_{bf}, Le, Nb, Nt, Nv, and Nc on the velocity, temperature, and the concentration profiles as well as the reduced Nusselt number and the heat transfer enhancement ratio are examined.

The variation of the surface temperature gradient, $-\theta'(0)$, for various values of the Prandtl number of the base fluid are presented in Table 1. When the Brownian motion parameter, thermophoresis parameter, and the variable viscosity and variable thermal conductivity parameters are chosen to be zero, the present study reduces to the boundary layer heat transfer of a conventional base fluid. In this case, a comparison between the present study and the works of Khan and Pop [11], Noghrehabadi et al. [16], Wang [40], and Gorla and Sidawi [41] is presented in Table 1. Moreover, as a comparison with previous studies, the velocity and temperature profiles are shown in Fig. 2 when $Pr_{bf} = 0.7$. To examine the accuracy of the current results for different values of variable thermal conductivity, see Fig. 3, in which the present results for the temperature profile are compared to the results, obtained by Noghrehabadi et al. [23], when the concentration of the nanoparticles at the surface of the sheet is constant ($C = C_w$). It is clear that the present results are in very good agreement with the previously published results in the literature.

As a practical case, the non-dimensional parameters are obtained for water as a base fluid and Al_2O_3 and Cu as the dispersed nanoparticles. The physical properties of water, Al_2O_3, and Cu are obtained from the literature [42, 43]. The magnitudes of the non-dimensional parameters (i.e., Pr_{nf}, Le, Nb, Nt, Nv, and Nc) are presented in Table 2. It is assumed that the nanoparticle volume fraction varies between 1% and 5%; two typical sizes of 10 and 50 nm are adopted for the diameters of the nanoparticles. Moreover, the reference temperature for calculating the Brownian motion parameter ($D_B = K_B T/3\pi\mu d_p$) is assumed to be equal to 300 K; the temperature difference in the thermophoresis parameter (see (16)) is adopted as 10 K. It is found that the ranges of the non-dimensional parameters are in agreement with the recent work by Noghrehabadi et al. [24, 44, 45] who discussed the practical ranges of the non-dimensional parameters of nanofluids.

The non-dimensional shear stress at the surface of the sheet ($f''(0)$), concentration of nanoparticles at the surface of the sheet ($\phi(0)$), reduced Nusselt number (Nur), and the heat transfer enhancement ratio (h_{nf}/h_{bf}) are displayed in Table 3. The results of Table 3 correspond to the calculated non-dimensional parameters

Table 1. Comparisons of results for temperature gradient $-\theta'(0)$.

Pr_{bf}	Present results	Khan and Pop [11]	Wang [40]	Gorla and Sidawi [41]
0.70	0.454048	0.4539	0.4539	0.4539
2.00	0.911357	0.9113	0.9114	0.9114
7.00	1.895404	1.8954	1.8954	1.8905
20.00	3.353905	3.3539	3.3539	3.3539
70.00	6.462197	6.4621	6.4622	6.4622

Fig. 2. Comparisons between the current results and the results that reported by Noghrehabadi et al. [16] and Wang [40] for velocity and temperature profiles.

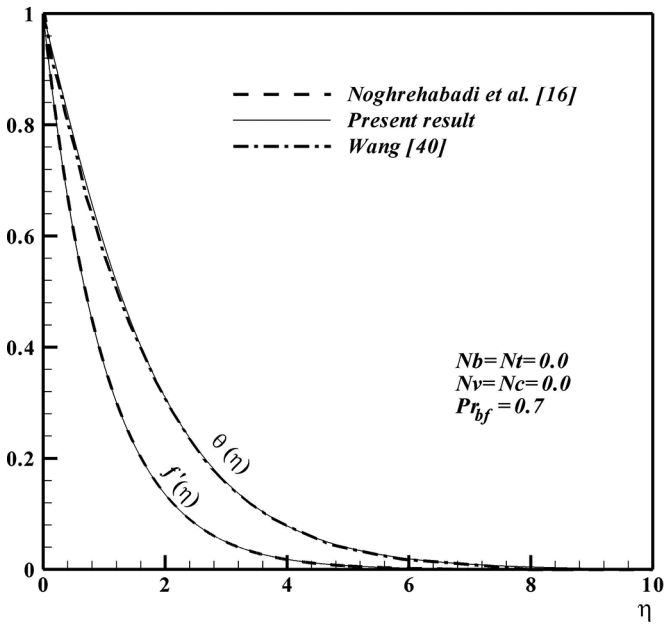

Fig. 3. Comparisons between the current results of temperature profile and the results that reported by Noghrehabadi et al. [23].

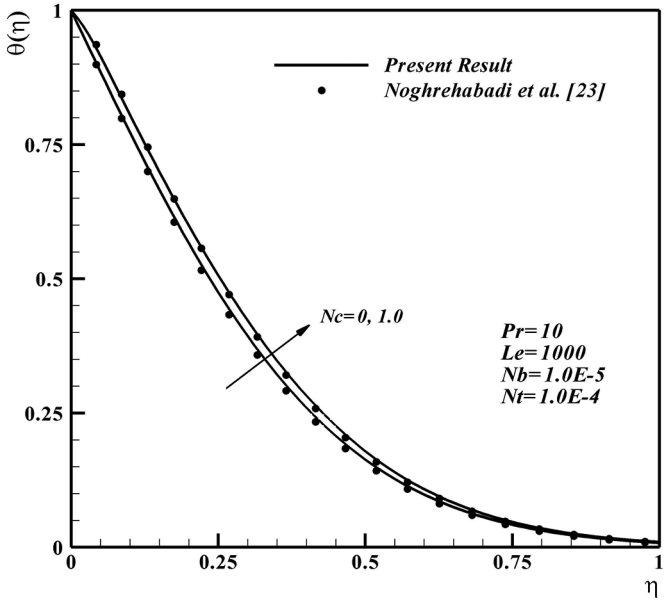

Table 2. Variation of non-dimensional parameters for various values of diameter and volume fraction of for Al_2O_3 and Cu as nanoparticles and water as the base fluid with Pr_{bf} = 6.835831.

	d_p (nm)	C_∞ (%)	Nc	Nv	Nb	Nt	Le	Pr_{nf}
Al_2O_3	10	1	0.02812	0.02481	3.0155×10^{-7}	9.4011×10^{-7}	24192.20	6.8126
Al_2O_3	10	3	0.08132	0.07332	9.1435×10^{-7}	2.8358×10^{-6}	24066.98	6.7767
Al_2O_3	10	5	0.13081	0.12035	1.5341×10^{-6}	4.7525×10^{-6}	24039.69	6.7545
Al_2O_3	50	1	0.02812	0.02481	6.0310×10^{-8}	9.4011×10^{-7}	120961.0	6.8126
Al_2O_3	50	3	0.08132	0.07332	1.8287×10^{-7}	2.8358×10^{-6}	120334.9	6.7769
Al_2O_3	50	5	0.13081	0.12035	3.0682×10^{-7}	4.7525×10^{-6}	120198.5	6.7545
Cu	10	1	0.02928	0.02481	3.5762×10^{-7}	1.0901×10^{-7}	23077.95	6.8045
Cu	10	3	0.08454	0.07332	1.1738×10^{-6}	3.2819×10^{-7}	21168.41	6.7531
Cu	10	5	0.13580	0.12035	2.1028×10^{-6}	5.4892×10^{-7}	19763.20	6.7158
Cu	50	1	0.02928	0.02481	7.1525×10^{-8}	1.0901×10^{-7}	115389.8	6.8045
Cu	50	3	0.08454	0.07332	2.3476×10^{-7}	3.2819×10^{-7}	105842.1	6.7531
Cu	50	5	0.13580	0.12035	4.2057×10^{-7}	5.4892×10^{-7}	98815.99	6.7158

Table 3. Alteration of dimensionless shear stress $f''(0)$, concentration $\phi(0)$, reduced Nusselt number Nur and enhancement ratio h_{nf}/h_{bf} for various values of diameter and volume fraction for Al_2O_3 and Cu as nanoparticles and water as the base fluid with Pr_{bf} = 6.835831.

	d_p (nm)	C_∞ (%)	$-f''(0)$	$-\phi(0)$	Nu_r	h_{nf}/h_{bf}
Al_2O_3	10	1	1.001141	4.61349×10^{-2}	1.866873	1.029138
Al_2O_3	10	3	1.003371	4.592065×10^{-2}	1.861398	1.088362
Al_2O_3	10	5	1.005533	4.584723×10^{-2}	1.857925	1.148834
Al_2O_3	50	1	1.002589	0.1041856	1.866875	1.029140
Al_2O_3	50	3	1.007661	0.1038185	1.861402	1.088364
Al_2O_3	50	5	1.012631	0.1037599	1.857929	1.148831
Cu	10	1	1.000115	4.611733×10^{-2}	1.865684	1.054283
Cu	10	3	1.000321	4.395413×10^{-3}	1.857761	1.162287
Cu	10	5	1.000507	4.231866×10^{-3}	1.852056	1.270331
Cu	50	1	1.000258	1.041124×10^{-2}	1.865677	1.054268
Cu	50	3	1.000729	9.927787×10^{-3}	1.857768	1.162291
Cu	50	5	1.001148	9.562217×10^{-3}	1.852053	1.270329

of Table 2. It is seen that an increase in the ambient volume fraction of nanoparticles, C_∞, causes decreases in the non-dimensional shear stress and the reduced Nusselt number. It is also clear that an augmentation of the ambient volume fraction of nanoparticles results in increasing the concentration of nanoparticles at the surface as well as the heat transfer enhancement ratio. The non-dimensional shear stress and the concentration of nanoparticles at the surface show a decreasing trend with the nanoparticle diameter for both Al_2O_3 and Cu. The effects of the nanoparticle diameter on the reduced Nusselt number and the heat transfer enhancement ratio are predicted to be negligible. It is clear that for larger diameters of nanoparticles (50 nm), the effect of increasing the ambient value of the volume fraction of nanoparticles on the non-dimensional shear stress is much higher than for smaller nanoparticles diameters. For example, in the case of Al_2O_3, when the nanoparticle diameter is 10 nm, the non-dimensional shear stress is changed about 0.0044 by increasing the volume fraction of nanoparticles from 1% to 5%; but, when the nanoparticle diameter is 50 nm, the non-dimensional shear stress is changed about 0.0100 by increasing the volume fraction of nanoparticles from 1% to 5%. Moreover, increasing the diameter of the nanoparticles is more effective on the concentration of nanoparticles at the surface of the sheet than increasing the ambient volume fraction of nanoparticles. For example, in the case of Al_2O_3, the concentration at the surface of the sheet is changed from -4.61×10^{-2} to -4.59×10^{-2} by increasing the volume fraction of nanoparticles from 1% to 5%; but, the concentration at the surface of the sheet is changed from -4.61×10^{-2} to −0.104 by increasing the diameter of the nanoparticles from 10 to 50 nm. The velocity, temperature, and concentration profiles for water–Al_2O_3 nanofluids with a 2.5% volume fraction of nanoparticles are plotted in Fig. 4. The reference temperature for calculating the Brownian motion parameter ($D_B = K_B T/3\pi\mu d_p$) is assumed to be equal to 300 K and the temperature difference in the thermophoresis parameter and nanoparticle diameter are considered to be 10 K and 10 nm, respectively. The corresponding values of the non-dimensional parameters are given in the figure. It is clear that the boundary layer thickness of the concentration profile is much smaller than those for the velocity and temperature profiles. The nanoparticle concentration, $\phi(0)$, at the surface of the sheet is computed to be equal to -4.596019×10^{-2}. The negative values of $\phi(0)$ show that the volume fraction of nanoparticles at the surface of the sheet is lower than the ambient values of the volume fraction of nanoparticles.

Figure 5 illustrates the effects of the Lewis number and the Prandtl number of the base fluid on the concentration profiles when the other parameters are fixed. An increase in the Prandtl number of the base fluid leads to a decrease in the thickness of the concentration boundary layer; however, the thickness of the concentration boundary layer is an increasing function of the Lewis number. Furthermore, when the Prandtl number of the base fluid increases from 5 to 7, the concentration of the nanoparticles at the surface of the sheet decreases from -1.9224×10^{-2} to -2.3148×10^{-2} in the case of $Le = 1.0\times10^4$. When the Lewis number increases from 1.0×10^4 to 5.0×10^4 in the case of Pr_{bf} = 5, the concentration of nanoparticles at the surface of the sheet increases from -1.9224×10^{-2} to -8.7023×10^{-3}. Accordingly, an augmentation in the Lewis number decreases the nanoparticle migration from the vicinity of the wall to the ambient. However, it is evident that an increase in the value of the Prandtl number of the base fluid tends to

Fig. 4. The velocity, temperature, and concentration profiles for water as base fluid and 2.5% of Al_2O_3 nanoparticle.

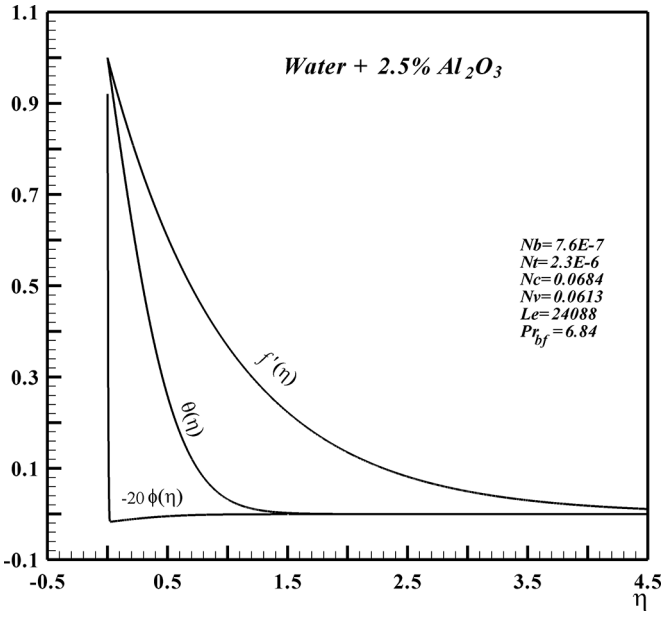

Fig. 5. Effects of Prandtl number of the base fluid and Lewis number on concentration profiles.

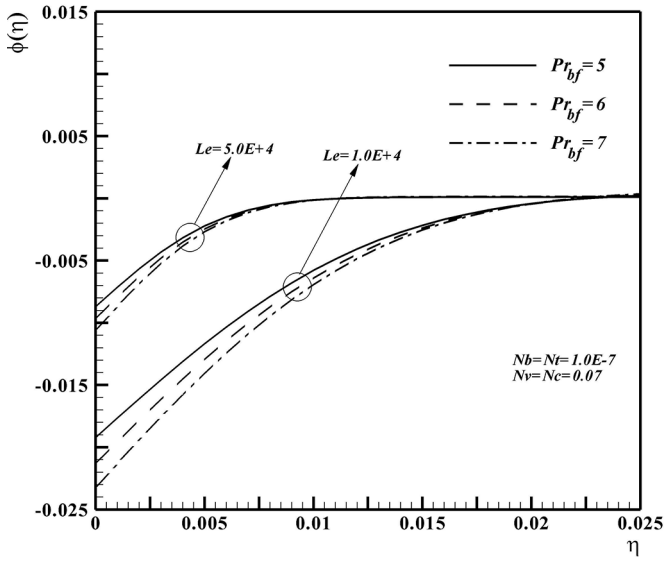

increase the migration of the nanoparticles from the vicinity of the wall to the ambient.

Figure 6 depicts the effects of the Brownian motion and the thermophoresis parameters on the concentration profiles. Increasing the thermophoresis parameter results in a decreasing concentration boundary layer thickness; however, the thickness of the concentration boundary layer increases by increasing the Brownian motion parameter. In addition, in the case of Nb = 1.0×10^{-7}, when the thermophoresis parameter increases from 5.0×10^{-7} to 1.0×10^{-6}, the concentration of nanoparticles at the surface of the sheet decreases from 0.106 502 9 to −0.213 409 6. This is because an augmentation of the thermophoresis parameter increases the migration of nanoparticles from hot regions to cold regions. In the present study, the surface is hot, and hence, the

Fig. 6. Effects of Brownian motion and thermophoresis parameters on concentration profiles.

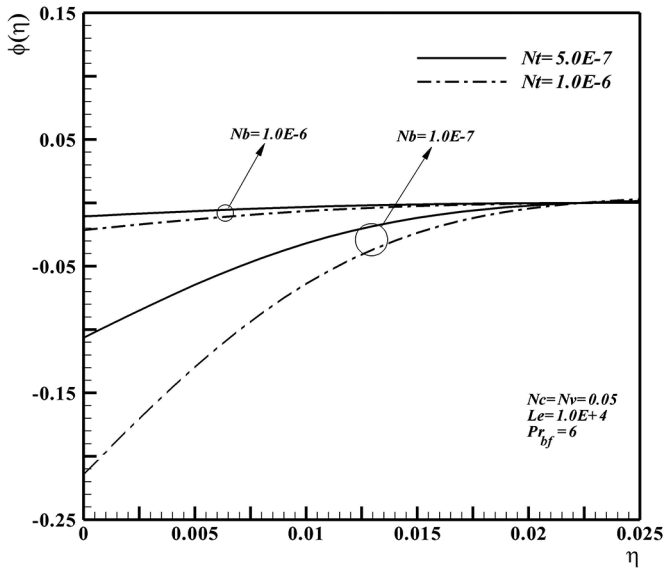

nanoparticles migrate from the surface of the sheet to the ambient region. In contrast, when the Brownian motion parameter increases from 1.0×10^{-7} to 1.0×10^{-6} for the case of Nt = 5.0×10^{-7}, the concentration of the nanoparticles at the surface of the sheet increases from −0.106 502 9 to $-1.063\ 225\ 1 \times 10^{-2}$. This is because increasing the Brownian motion parameter results in increasing the nanoparticle migration from the high concentration regions to the regions with low concentration. Furthermore, Fig. 5 clearly shows that the effects of altering the thermophoresis parameter on the changes of the concentration profiles are much higher for low values of the Brownian motion parameter (Nb = 1.0×10^{-7}) than for high values of the Brownian motion parameter (Nb = 1.0×10^{-6}).

The effects of the Brownian motion and the thermophoresis parameters on the reduced Nusselt number are shown in Fig. 7. This figure shows that the reduced Nusselt number is a decreasing function of the thermophoresis parameter. However, it is an increasing function of the Brownian motion parameter. Moreover, it is clear that increasing the Brownian motion parameter leads to decreasing the effects of the thermophoresis parameter. It is worth noticing that increasing the Brownian motion parameter tends to increase the nanoparticle concentration in the vicinity of the wall, and this increase raises the heat transfer rate from the surface. Augmentation of the thermophoresis parameter reduces the number of nanoparticles in the vicinity of the sheet. Accordingly, this leads to a decrease in the heat transfer rate from the sheet.

Figure 8 depicts the effects of variable thermal conductivity parameter and Prandtl number of the base fluid on the reduced Nusselt number. It is obvious that when the variable thermal conductivity increases, the reduced Nusselt number declines. On the other hand, the increase of the Prandtl number of the base fluid increases the reduced Nusselt number. According to (19), increasing variable thermal conductivity Nc shows a direct effect on the reduced Nusselt number and also contributes to alteration in the temperature profile and $\theta'(0)$; hence, the Prandtl number of the base fluid has only indirect effects on the reduced Nusselt number. Augmentation in the Prandtl number of the base fluid causes an alteration in $\theta'(0)$; consequently, the reduced Nusselt number increases.

Fig. 7. Effects of Brownian motion and thermophoresis parameters on reduced Nusselt number.

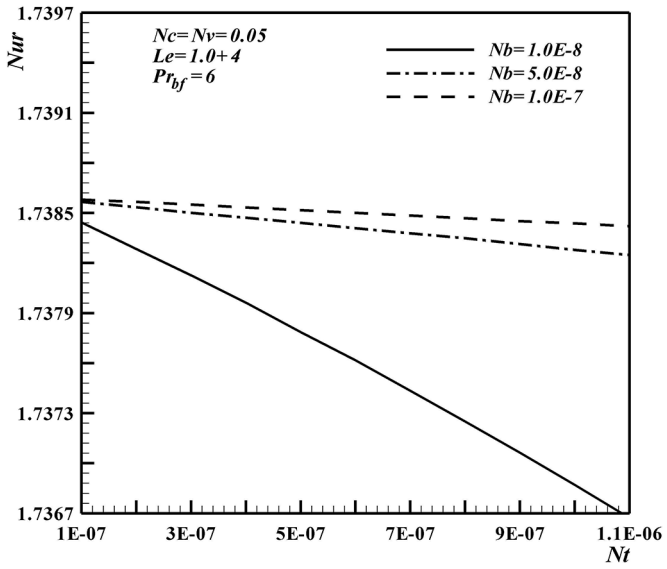

Fig. 8. Effects of variable thermal conductivity and Prandtl number of base fluid on reduced Nusselt number.

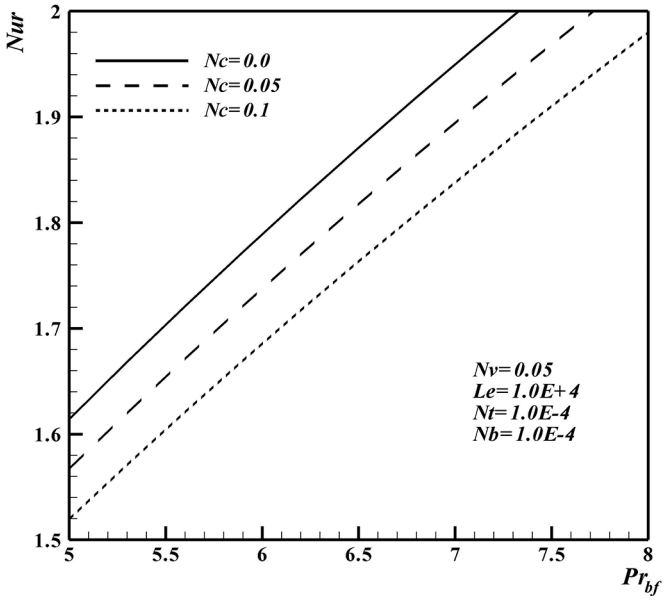

Fig. 9. Effects of Brownian motion and thermophoresis parameters on enhancement ratio.

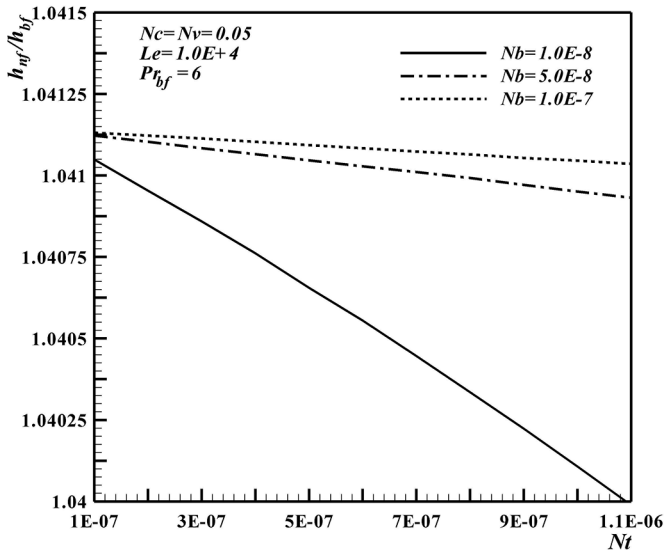

Fig. 10. Effects of variable thermal conductivity and variable viscosity parameters on enhancement ratio.

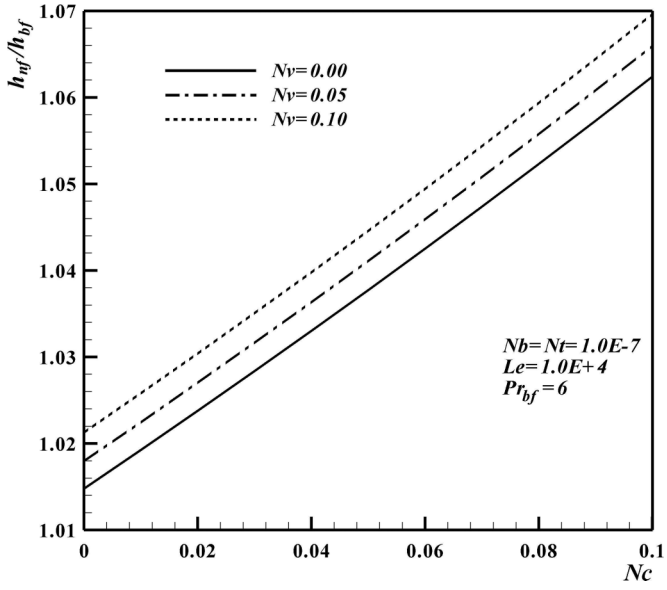

Figure 9 illustrates the effects of the Brownian motion and the thermophoresis parameters on the heat transfer enhancement ratio when the other parameters are fixed. It is found that the heat transfer enhancement ratio is a decreasing function of the thermophoresis parameter, but is an increasing function of the Brownian motion, which is the same as the result for the reduced Nusselt number, presented in Fig. 7. Increasing the Brownian motion parameter has the tendency to increase the nanoparticle migration from dense regions to dilute regions. This increase in the migration of nanoparticles increases the nanoparticle concentration in the vicinity of the wall, and hence augments the wall heat transfer rate.

The effects of the variable viscosity and the variable thermal conductivity parameters on the heat transfer enhancement ratio are plotted in Fig. 10. The heat transfer enhancement ratio increases when either the variable thermal conductivity parameter or the variable viscosity parameter increases. Using (8) and (9), the thermal conductivity and the viscosity of the base fluid can be approximated as $k_{nf,\infty} = k_{bf}/(1 - Nc)$ and $\mu_{nf,\infty} = \mu_{bf}/(1 - Nv)$, respectively, when $C = 0$. It is clear that an increase in the value of Nc (or Nv) raises the thermal conductivity (or the dynamic viscosity) of the nanofluid. Increasing the variable thermal conductivity parameter tends to directly increase the heat transfer rate because of the increase in the overall thermal conductivity. However, it should be noted that increasing Nc also induces indirect effects on the wall heat transfer rate through alteration of the temperature gradient $\theta'(0)$ as well as the thermal conductivity of the nanofluid ($k_{w,nf}$) near the sheet. Moreover, by increasing the variable viscosity parameter, the nanofluid would act as a fluid with a high viscosity compared to the base fluid. Hence, the velocity perco-

lates more in the boundary layer. This is because the velocity and the hydrodynamic boundary layer originate from the stretching of the sheet while the ambient is quiescent. As the velocity increases in the boundary layer, the flow can transfer more heat through the boundary layer. Although it is clear that any increase in the value of Nv causes an increase in the viscosity of the nanofluid in comparison with the base fluid, increasing Nv alters the non-dimensional sheer stress ($f''(0)$) as well as the viscosity of the nanofluid in the vicinity of the sheet (μ_w). In all studied cases, the heat transfer enhancement ratio is greater than unity. This indicates that dispersing nanoparticles in the base fluid enhances the wall heat transfer rate.

4. Conclusion

The boundary layer flow and heat transfer of nanofluids over an isothermal impermeable stretching sheet is investigated. A practical boundary condition, zero mass flux of nanoparticles through the sheet, for the concentration boundary layer of nanoparticles is assumed. The effect of the local volume fraction of nanoparticles on the thermal conductivity and the dynamic viscosity of the nanofluid is taken into account using a linear approximation. The governing partial differential equations are reduced to ordinary differential equations. An enhancement ratio parameter is proposed to compare the convective heat transfer coefficient of the nanofluid (h_{nf}) with the base fluid (h_{bf}). The practical ranges of the non-dimensional parameters, namely, the Prandtl number of the nanofluid Pr_{nf}, Lewis number Le, Brownian motion parameter Nb, thermophoresis parameter Nt, variable thermal conductivity parameter Nc, and the variable viscosity parameter Nv are discussed. The most important findings of the present study can be summarized as follows.

1. An increase in the ambient value of the volume fraction of nanoparticles for both nanofluids, Al_2O_3–water and Cu–water, results in decreasing the non-dimensional shear stress $f''(0)$ and the reduced Nusselt number Nur. Furthermore, increasing the ambient values of the volume fraction of nanoparticles produces increases in the concentration of the nanoparticles at the surface ϕ (0) as well as the heat transfer enhancement ratio h_{nf}/h_{bf}.
2. The non-dimensional shear stress and the concentration of nanoparticles at the surface for both Al_2O_3–water and Cu–water nanofluids are decreasing functions of the nanoparticle diameter. In addition, the effects of the nanoparticle diameter on the reduced Nusselt number and the enhancement ratio are found to be negligible.
3. The concentration of nanoparticles at the surface of the sheet decreases as the Prandtl number of the base fluid increases. However, the concentration of nanoparticles at the surface of the sheet is an increasing function of the Lewis number.
4. As the thermophoresis parameter is raised, the concentration of nanoparticles at the surface of the sheet declines. In contrast, as the Brownian motion parameter increases, the concentration of nanoparticles at the surface of the sheet increases.
5. The reduced Nusselt number and the heat transfer enhancement ratio are decreasing functions of the thermophoresis parameter; however, they are increasing functions of the Brownian motion.
6. An augmentation of the variable viscosity and the variable thermal conductivity parameters causes the heat transfer enhancement ratio to increase.
7. The reduced Nusselt number is affected by the Prandtl number of the base fluid and the variable thermal conductivity parameter. Increasing the Prandtl number of the base fluid results in increases in the reduced Nusselt number; in contrast, the reduced Nusselt number decreases as a result of the augmentation in the variable thermal conductivity parameter.

References

1. Z. Tadmor and I. Klein. Engineering principles of plasticating extrusion. Van Nostrand Reinhold, New York. 1970.
2. E.G Fisher. Extrusion of plastics. Wiley, New York. 1976.
3. T. Altan, S.I. Oh, and H.L. Gegel. Metal forming: fundamentals and applications. *In* ASM Series in Metal Processing. Vol. 1. American Society for Metals, Materials Park, OH. 1983.
4. L.J. Crane and Z. Angew. Math. Phys. **21**, 645 (1970). doi:10.1007/BF01587695.
5. J.A. Eastman, S.U.S. Choi, S. Li, W. Yu, and L.J. Thompson. Appl. Phys. Lett. **78**, 718 (2001). doi:10.1063/1.1341218.
6. S.K. Das, S.U.S. Choi, W. Yu, and T. Pradeep. Nanofluids: science and technology. John Wiley & Sons, Hoboken, NJ. 2007.
7. X.Q. Wang and A.S. Mujumdar. Braz. J. Chem. Eng. **25**, 613 (2008). doi:10.1590/S0104-66322008000400001.
8. S. Kakaç and A. Pramuanjaroenkij. Int. J. Heat Mass Transfer, **52**, 3187 (2009). doi:10.1016/j.ijheatmasstransfer.2009.02.006.
9. M. Chandrasekar, S. Suresh, and T. Senthilkumar. Renewable Sustainable Energy Rev. **16**, 3917 (2012). doi:10.1016/j.rser.2012.03.013.
10. J.M. Wu and J. Zhao. Prog. Nucl. Energy, **66**, 13 (2013). doi:10.1016/j.pnucene.2013.03.009.
11. W.A. Khan and I. Pop. Int. J. Heat Mass Transfer, **53**, 2477 (2010). doi:10.1016/j.ijheatmasstransfer.2010.01.032.
12. M. Hassani, M.M. Tabar, H. Nemati, G. Domairry, and F. Noori. Int. J. Therm. Sci. **50**, 2256 (2011). doi:10.1016/j.ijthermalsci.2011.05.015.
13. M.D.S. Khan, M.D.M. Alam, and M. Ferdows. *In* Proceedings of the International Conference on Mechanical Engineering and Renewable Energy, 22–24 December 2011, Chittagong, Bangladesh. 2011.
14. O.D. Makinde and A. Aziz. Int. J. Therm. Sci. **50**, 1326 (2011). doi:10.1016/j.ijthermalsci.2011.02.019.
15. P. Rana and R. Bhargava. Commun. Nonlinear. Sci. Numer. Simul. **17**, 212 (2012). doi:10.1016/j.cnsns.2011.05.009.
16. A. Noghrehabadi, R. Pourrajab, and M. Ghalambaz. Int. J. Therm. Sci. **54**, 253 (2012). doi:10.1016/j.ijthermalsci.2011.11.017.
17. A. Noghrehabadadi, M. Ghalambaz, and A. Ghanbarzadeh. J. Thermophys. Heat. Transfer, **26**, 686 (2012). doi:10.2514/1.T3866.
18. A. Noghrehabadi, R. Pourrajab, and M. Ghalambaz. Heat Mass Transfer, **49**, 1357 (2013). doi:10.1007/s00231-013-1179-y.
19. A. Noghrehabadi, M.R. Saffarian, R. Pourrajab, and M. Ghalambaz. J. Mech. Sci. Technol. **27**, 927 (2013). doi:10.1007/s12206-013-0104-0.
20. S. Nadeem, R. Mehmood, and N.S. Akbar. Int. J. Heat Mass Transfer, **57**, 679 (2013). doi:10.1016/j.ijheatmasstransfer.2012.10.019.
21. S. Nadeem, R.U. Haq, N.S. Akbar, C. Lee, and Z.H. Khan. PLoS ONE, **8**, e69811 (2013). doi:10.1371/journal.pone.0069811.
22. B. Jalilpour, S. Jafarmadar, D.D. Ganji, A.B. Shotorban, and H. Taghavifar. J. Mol. Liq. **195**, 194 (2014). doi:10.1016/j.molliq.2014.02.021.
23. A. Noghrehabadi, E. Izadpanahi, and M. Ghalambaz. Comput. Fluids, **100**, 227 (2014). doi:10.1016/j.compfluid.2014.05.013.
24. A. Noghrehabadi, M. Ghalambaz, and A. Ghanbarzadeh. J. Mech. **30**, 265 (2014). doi:10.1017/jmech.2013.61.
25. A.V. Kuznetsov and D.A. Nield. Int. J. Heat Mass Transfer, **65**, 682 (2013). doi:10.1016/j.ijheatmasstransfer.2013.06.054.
26. M.M. Rahman, A.V. Roşca, and I. Pop. Int. J. Heat Mass Transfer, **77**, 1133 (2014). doi:10.1016/j.ijheatmasstransfer.2014.06.013.
27. R.U. Haq, S. Nadeem, Z.H. Khan, and N.S. Akbar. Phys. E (Amsterdam, Neth.), **65**, 17 (2015). doi:10.1016/j.physe.2014.07.013.
28. J. Buongiorno. J. Heat Transfer, **128**, 240 (2006). doi:10.1115/1.2150834.
29. M. Chandrasekar and S. Suresh. Heat Transfer Eng. **30**, 1136 (2009). doi:10.1080/01457630902972744.
30. K. Khanafer and K. Vafai. Int. J. Heat Mass Transfer, **54**, 4410 (2011). doi:10.1016/j.ijheatmasstransfer.2011.04.048.
31. J.H. Lee, K.S. Hwang, S.P. Jang, B.H. Lee, J.H. Kim, S.U.S. Choi, and C.J. Choi. Int. J. Heat Mass Transfer, **51**, 2651 (2008). doi:10.1016/j.ijheatmasstransfer.2007.10.026.
32. H.A. Mintsa, G. Roy, C.T. Nguyen, and D. Doucet. Int. J. Therm. Sci. **48**, 363 (2009). doi:10.1016/j.ijthermalsci.2008.03.009.
33. R.S. Vajjha and D.K. Das. Int. J. Heat Mass Transfer, **52**, 4675 (2009). doi:10.1016/j.ijheatmasstransfer.2009.06.027.
34. M. Chandrasekar, S. Suresh, and A. Chandra Bose. Exp. Therm. Fluid Sci. **34**, 210 (2010). doi:10.1016/j.expthermflusci.2009.10.022.
35. M. Jahanshahi, S.F. Hosseinizadeh, M. Alipanah, A. Dehghani, and G.R. Vakilinejad. Int. Commun. Heat Mass Transfer, **37**, 687 (2010). doi:10.1016/j.icheatmasstransfer.2010.03.010.
36. P.K. Namburu, D.P. Kulkarni, D. Misra, and D.K. Das. Exp. Therm. Fluid Sci. **32**, 397 (2007). doi:10.1016/j.expthermflusci.2007.05.001.
37. C.T. Nguyen, F. Desgranges, N. Galanis, G. Roy, T. Maré, S. Boucher, and H.A. Mintsa. Int. J. Therm. Sci. **47**, 103 (2008). doi:10.1016/j.ijthermalsci.2007.01.033.
38. J. Buongiorno, D.C. Venerus, N. Prabhat, et al. J. Appl. Phys. **106**, 094312 (2009). doi:10.1063/1.3245330.
39. D.C. Venerus, J. Buongiorno, et al. Appl. Rheol. **20**, 44582 (2010). doi:10.3933/ApplRheol-20-44582.
40. C.Y. Wang. Z. Angew. Math. Mech. **69**, 418 (1989). doi:10.1002/zamm.19890691115.

41. R.S.R. Gorla and I. Sidawi. Appl. Sci. Res. **52**, 247 (1994). doi:10.1007/BF00853952.
42. M. Hatami, R. Nouri, and D.D. Ganji. J. Mol. Liq. **187**, 294 (2013). doi:10.1016/j.molliq.2013.08.008.
43. M. Hatami, M. Sheikholeslami, and D.D. Ganji. J. Mol. Liq. **195**, 230 (2014). doi:10.1016/j.molliq.2014.02.024.
44. A. Noghrehabadi and A. Behseresht. Comput. Fluids, **88**, 313 (2013). doi:10.1016/j.compfluid.2013.09.019.
45. A. Behseresht, A. Noghrehabadi, and M. Ghalambaz. Chem. Eng. Res. Des. **92**, 447 (2014). doi:10.1016/j.cherd.2013.08.028.

List of symbols

a	constant
C	nanoparticle volume fraction
D_B	Brownian diffusion coefficient
D_T	thermophoretic diffusion coefficient
k	thermal conductivity
Le	Lewis number
Nb	Brownian motion parameter
Nc	variable thermal conductivity parameter
Nt	thermophoresis parameter
Nv	variable viscosity parameter
Nur	reduced Nusselt number
Pr	Prandtl number
q_w	wall Heat flux
Re_x	Reynolds number
T	temperature
u, v	velocity components along x and y-axes
x, y	physical coordinates (x-axis is aligned along the stretching sheet and y-axis is normal to it)
α	thermal diffusivity
$\phi(\eta)$	concentration of nanoparticles
η	similarity variable
$\theta(\eta)$	dimensionless temperature
υ	kinematic viscosity of nanofluid
ρc	heat capacity
ρ	density
ψ	stream function

Subscripts

bf	base fluid
nf	nanofluid
p	nanoparticles
w	values at the wall
∞	ambient value